iScience

CellPress
OPEN ACCESS

Article

Engineering of thick human functional myocardium via static stretching and electrical stimulation

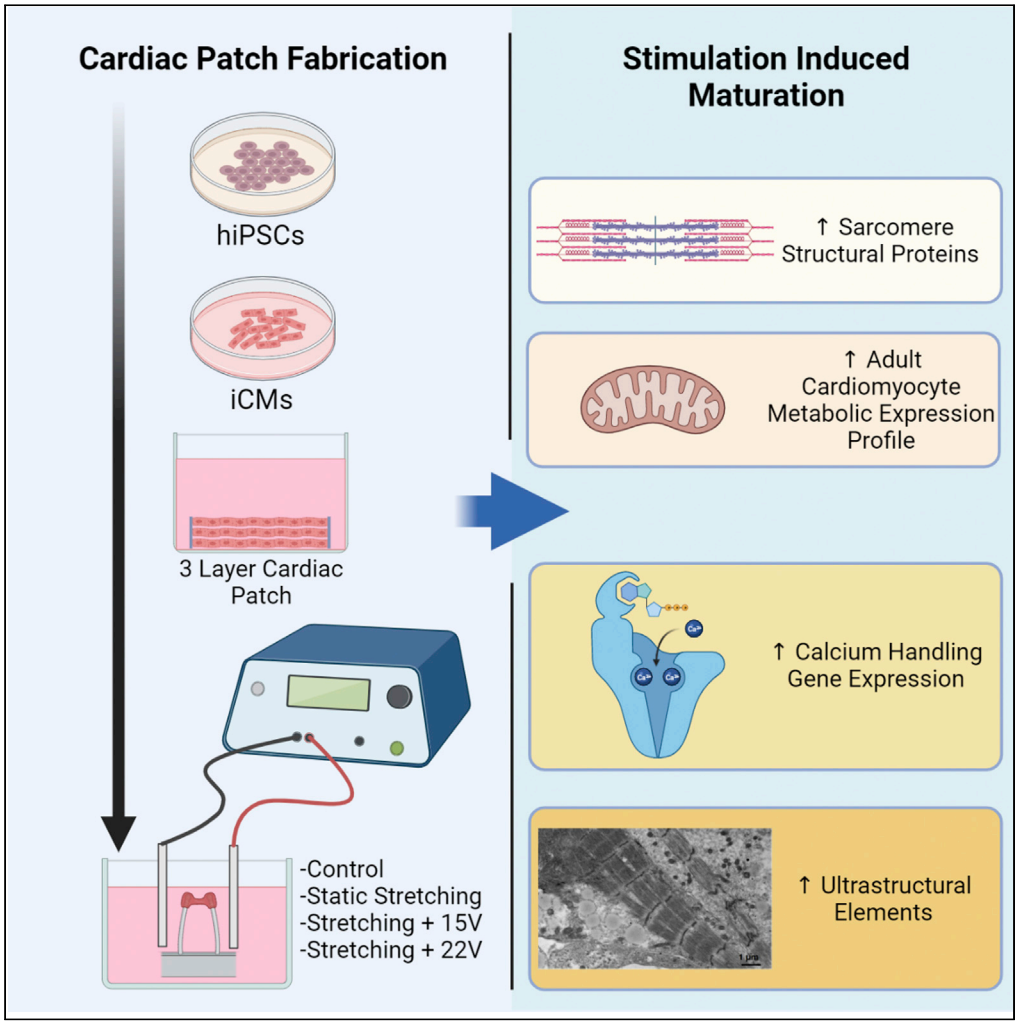

Danielle Pretorius, Asher M. Kahn-Krell, Wesley C. LaBarge, Xi Lou, Jianyi Zhang

jayzhang@uab.edu

Highlights

Thick (>2.1 mm) triple-layered hCMPs were constructed using layer-by-layer fabrication

Combined stretching and electrical stimulation improve hCMP biochemical maturation

Increased ultrastructural components were promoted by all stimulation methods

Pretorius et al., iScience 25, 103824
March 18, 2022
https://doi.org/10.1016/j.isci.2022.103824

iScience

CellPress
OPEN ACCESS

Article

Engineering of thick human functional myocardium via static stretching and electrical stimulation

Danielle Pretorius,[1,3] Asher M. Kahn-Krell,[1,3] Wesley C. LaBarge,[1] Xi Lou,[1] and Jianyi Zhang[1,2,4,*]

SUMMARY

Human cardiac-muscle patches (hCMPs) constructed from induced pluripotent stem cells derived cardiomyocytes (iCMs) can replicate the genetics of individual patients, and consequently be used for drug testing, disease modeling, and therapeutic applications. However, conventional hCMPs are relatively thin and contain iCMs with fetal cardiomyocyte structure and function. Here, we used our layer-by-layer (lbl) fabrication to construct thicker (>2.1 mm), triple-layered hCMPs, and then evaluated iCM maturity after ten days of standard culture (Control), static stretching (Stretched), or stretching with electrical stimulation at 15 or 22 V (Stretched+15V or Stretched+22V). Assessments of stained hCMPs suggested that expression and alignment of contractile proteins was greater in Stretched+22V, whereas quantification of mRNA abundance and protein expression indicated the Stretched+22V enhanced biomolecular maturation. Transmission electron microscope images indicated that stretching and electrical stimulation were associated with increases in development of Z-lines and gap junctions, and sarcomeres were significantly longer following any of the maturation protocols.

INTRODUCTION

Disease modeling and drug testing have historically been conducted primarily in animal models (Hartung, 2008). However, the development of techniques for generating tissues from human induced pluripotent stem cells (hiPSCs) has enabled researchers to conduct *in vitro* experiments on an entirely human platform (Argentati et al., 2020; Molinari and Sayer, 2020). Furthermore, because hiPSCs can be reprogrammed from each patient's own somatic cells, cardiomyocytes (CMs) differentiated from hiPSCs fully reproduce all the genetic factors that may influence the etiology and progression of heart disease in an individual patient, as well as the patient's response to treatment (Benam et al., 2015). Nevertheless, conventional fabrication techniques typically produce human cardiac muscle patches (hCMPs) that are relatively thin, and hiPSC-CMs are structurally and functionally more similar to CMs from fetal and neonatal hearts than from the hearts of adults, which has deterred both the investigational and therapeutic use of engineered hiPSC-derived cardiac tissues.

Numerous attempts have been made, to various degrees of success, to enhance the maturity of hiPSC-CMs (Scuderi and Butcher, 2017; Jiang et al., 2018). In many cases, the strategies have been based on one of the following aspects: electrical stimulation, mechanical stimulation, tailoring the 3D extracellular environment, or mimicking cell signaling by using small molecules or chemical agents. Each of these techniques mimics some type of activity which occurs in the normal cardiac environment (Karbassi et al., 2020). For example, during the continuous, normal pumping of the heart, an electrical signal is first propagated throughout the tissue because of the firing of special pacemaker cells, causing changes in ion concentrations inside and outside the cells (Grant, 2009). These differences in concentrations trigger an action potential in different areas of the heart as the signal travels to the various chambers, leading to contraction and stretching of the heart tissue (Bartos et al., 2015). To recapitulate this process, we can develop an optimized, concerted balance between electrical and mechanical stimuli, aided by the extracellular matrix (ECM) composition of the surrounding environment, which would in turn support physiologically relevant cell signaling cascades.

[1]Department of Biomedical Engineering, School of Medicine and School of Engineering, University of Alabama at Birmingham, Birmingham, AL 35233, USA

[2]Department of Medicine, Division of Cardiovascular Diseases, School of Medicine, University of Alabama at Birmingham, Birmingham, AL 35233, USA

[3]These authors contributed equally

[4]Lead contact

*Correspondence: jayzhang@uab.edu

https://doi.org/10.1016/j.isci.2022.103824

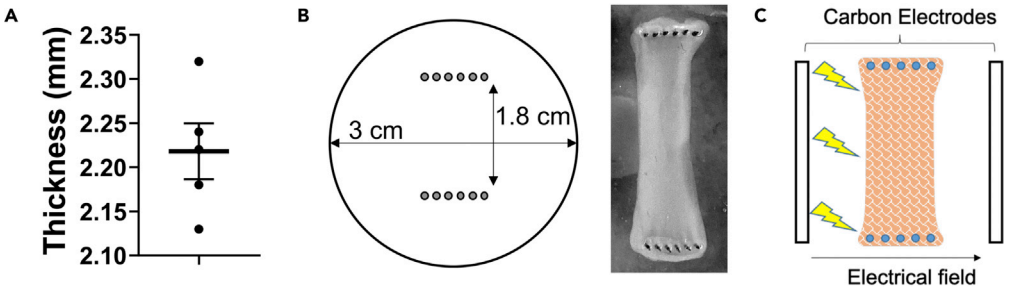

Figure 1. hCMPs were matured via static stretching with or without electrical stimulation

hCMPs were assembled in three layers over a three-day period (one layer per day) and then cultured for one week before maturation.

(A) hCMP thicknesses were measured before maturation.

(B and C) One week after fabrication, hCMPs were cultured under standard conditions (i.e., without stretching or electrical stimulation), (B) while stretched between two lines of needles, or (C) with stretching and electrical stimulation. Electrical stimulation was applied in 2-ms pulses at 2 Hz and either 15 V or 22 V

Both active and passive mechanical stimulation (Tulloch et al., 2011; Hirt et al., 2012; Mihic et al., 2014; Rogers et al., 2016; Ruan et al., 2016; Leonard et al., 2018), simulating the various loading phenomena observed in the heart, as well as highly controlled regimens of chronic, electrical stimulation (Tandon et al., 2009, 2011; Nunes et al., 2013; Hirt et al., 2014; Eng et al., 2016) have been employed, each showing promising improvements to structural or functional aspects of hiPSC-CM development. In addition, 3D engineering of the ECM environment has also aided in maturation by providing a structured environment for the cells to both efficiently connect and communicate while also providing a means for them to organize more akin to what is observed in adult heart tissue (Jung et al., 2016; Mills et al., 2017; Hall and Ogle, 2018).

Here we utilized passive mechanical stimulation along with chronic biphasic electrical stimulation (C-Pace, IonOptix) (Berger et al., 1994; Ivester et al., 1993; Kato et al., 1995) over a 10 day period, half of the time utilized by Ronaldson-Bouchard et al. (2018) to enhance the maturation of the hiPSC-CMs as well as the tissue overall. With our layer-by-layer (lbl) assembly technique we constructed thick (>2mm), triple-layered hCMPs from a solution of hiPSC-CMs in fibrin, and then investigated whether the maturity of the hCMPs could be enhanced by a regimen of passive stretching and electrical stimulation in combination.

RESULTS

Fabrication and stimulation of tri-layered patch

The thicknesses of the lbl-manufactured hCMPs following fabrication, before any maturation treatments, ranged from 2.1 to 2.3 mm (mean: 2.22 $\pm$ 0.03 mm; n = 5) (Figure 1A). One week after fabrication, the hCMPs were cultured for 10 days under standard maintenance conditions (the Control group), while stretched between two lines of needles (the Stretched group) (Figure 1B), with stretching and low-voltage (15 V) electrical stimulation (the Stretched+15V group), or with stretching and high-voltage (22 V) stimulation (the Stretched+22V group) (Figure 1C), n = 4 in each group; electrical stimulation was applied in 2-ms pulses at a frequency of at 2 Hz.

Maturation techniques improve fiber alignment and structural components

Qualitative assessments of immunofluorescent stained whole-mount hCMPs suggested that the expression and alignment of contractile proteins (cTnT and sarcomeric α-actinin) was greater in Stretched+22V hCMPs than in hCMPs from any other group (Figure 2). Close examination of fluorescently stained sarcomere proteins indicates fibers aligning in the direction of stretching and perpendicular to the electrical pulse. Furthermore, measurements of mRNA and protein abundance (Figures 3 and 5) identified changes in patterns of sarcomere gene expression and isoform switching, suggesting the Stretched+22V protocol significantly enhanced hCMP maturation. Declines in the expression of α myosin heavy chain (α-MHC) coupled with slight increases in levels of β-myosin heavy chain (β-MHC) resulted in increased mRNA and protein isoform switching ratios of 2.42 $\pm$ 0.71 and 2.36 $\pm$ 0.79, respectively, for the high voltage

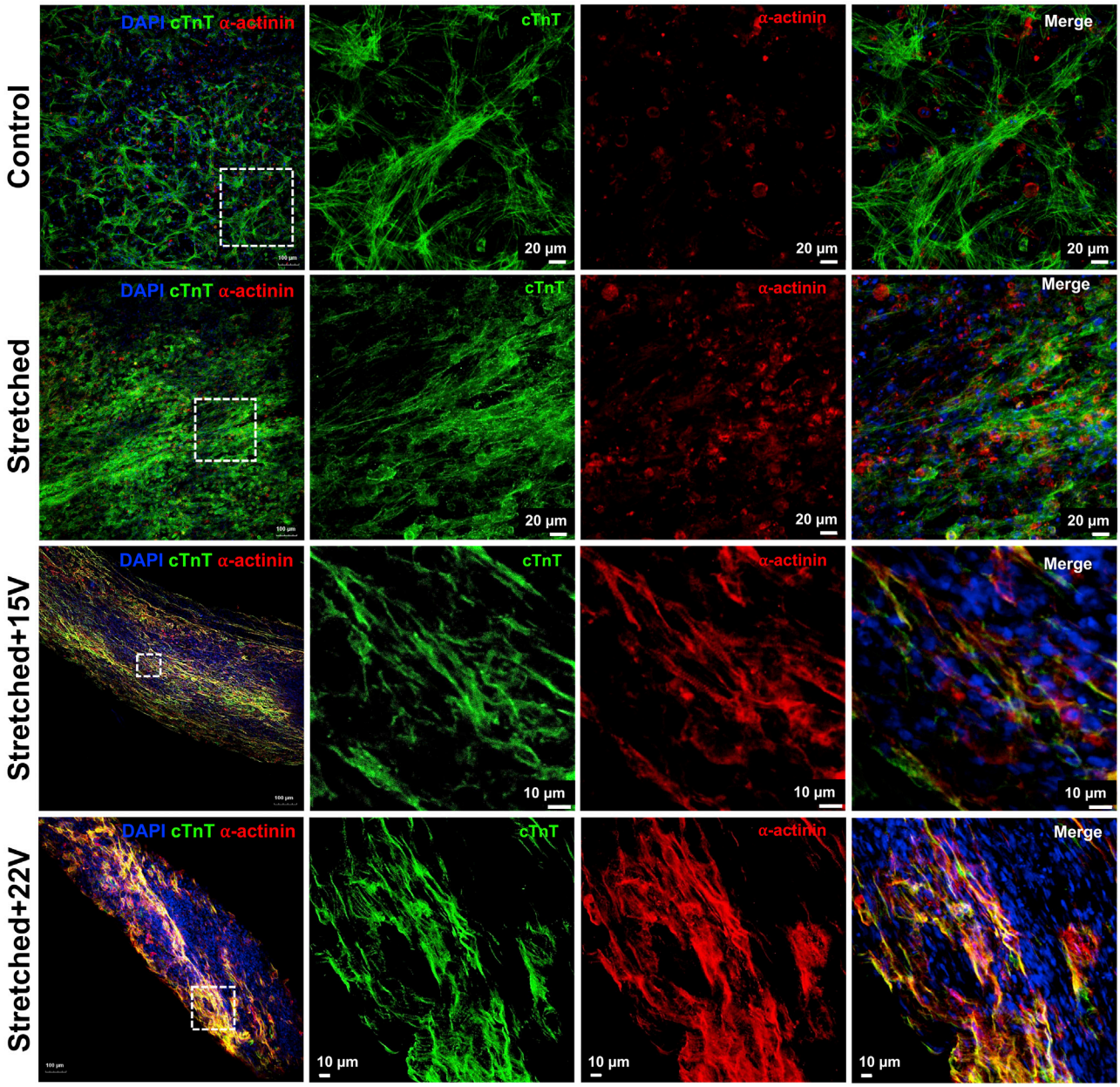

Figure 2. Static stretching with electrical stimulation was associated with more mature patterns of contractile protein expression

After 10 days of culture under standard conditions (i.e., in the absence of stretching or electrical stimulation; Control), with stretching alone (Stretched), or with stretching and either 15 V (Stretched+15V) or 22 V (Stretched+22V) electrical stimulation, contractile proteins were visualized in whole-mounted hCMPs via immunofluorescent staining for the expression of cTnT and α-actinin; nuclei were counterstained with DAPI

sample vs 1.14 ± 0.34 and 1.80 ± 0.83, respectively, for control. This change has been linked to improvements in contractile strength and a more adult phenotype (Allen and Leinwand, 2001; Reiser et al., 2001). A downregulation of myosin light-chain (MLC) 2a mRNA levels accompanied by an increase in the MLC2v:MLC2a ratio from 1.10 ± 0.31 to 1.86 ± 0.75 was also observed, which suggest that the hiPSC-CMs switched from an atrial to a ventricular phenotype (Ng et al., 2010; Goldfracht et al., 2020). The final structural protein examined that undergoes isoform switching during maturation and plays a key role in sarcomere function is Troponin I which has been offered as a useful marker for the fetal to adult cardiomyocyte transition (Bedada et al., 2014). When treated with dual stimulation, protein levels for TNNI 1 (3.06 ± 1.04) and TNNI 3 (2.05 ± 0.78) were both significantly increased over control patches

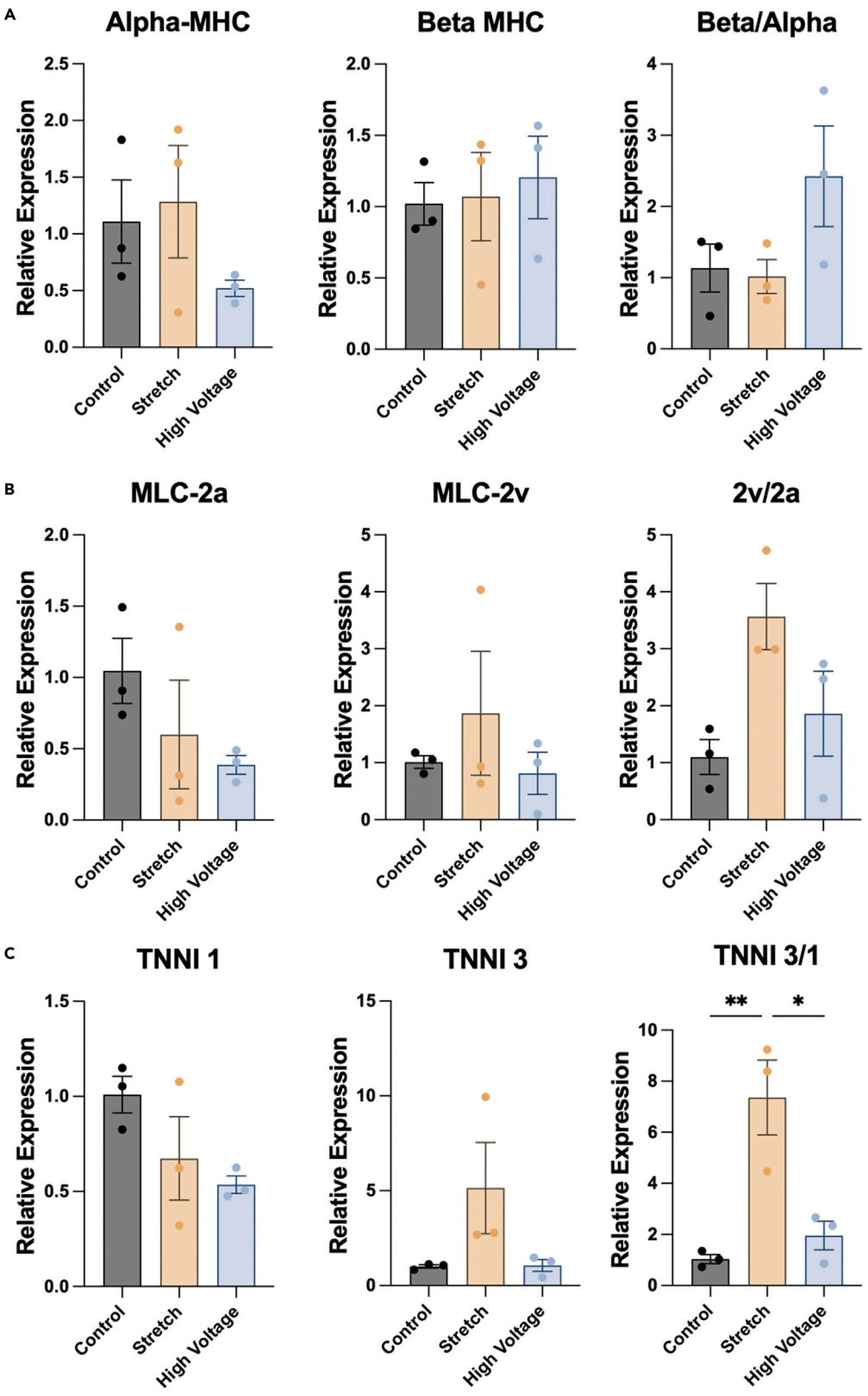
A
Alpha-MHC
Beta MHC
Beta/Alpha
Relative Expression
Control
Stretch
High Voltage
B
MLC-2a
MLC-2v
2v/2a
C
TNNI 1
TNNI 3
TNNI 3/1
**
*

Figure 3. Static stretching with 22-V electrical stimulation was associated with isoform switching of genes related to structural maturity

The relative mRNA expression of maturation genes and their isoform ratios of (A) Myosin Heavy Chain Alpha and Beta, (B) Myosin Light Chain Atrial and Ventricular, and (C) Troponin I one and three were evaluated in Control, Stretched, and Stretched+22V hCMPs via qPCR; results were normalized to the abundance of GAPDH mRNA in each sample (*$p < 0.05$, **$p < 0.01$; $n = 3$ per group).

(0.62 ± 0.15 and 0.01 ± 0.001, respectively). This could possibly be explained by the increased need for contractile proteins in the more rapidly and forcefully beating stimulated patch. Further, when the protein proportions of the isoforms were compared, the treated patch had a relative ratio of 0.71 ± 0.13 which was significantly higher than the level in the control patch of 0.01 ± 0.003. This expression pattern was less clearly defined when the mRNA was examined; however, this may be because of translational effects and transient fluctuations captured in mRNA analysis. Because the protein concentrations provide a greater representation of the functional status in the cells this result strongly suggests improved maturation with the stimulation regimen.

Electromechanical coupling and metabolic gene expression is highly influenced by stimulation

mRNA levels (Figure 4) indicate significant upregulation of genes involved in electromechanical coupling particularly N-cadherin (Bian et al., 2014; Lou et al., 2020). This result was confirmed with protein analysis showing relative levels of 5.93 ± 1.19 with dual treatment compared with 3.92 ± 0.72 in the control. Interestingly when the calcium handling gene HCN4 (Liu et al., 2009; Li et al., 2017; Jiang et al., 2018) was examined the mRNA levels were upregulated in the treated patch; however, the protein levels were significantly decreased (Control:11.83 ± 0.73; Stimulated:1.96 ± 0.62). A complete understanding of this discrepancy requires further examination but could possibly be explained by biological processes including different degradation timeframes of proteins and mRNA or posttranscriptional modifications resulting in decreased translation (Buccitelli and Selbach, 2020). Because HCN4 has been established as a crucial channel involved in the cardiac pacing process (Darche et al., 2019) the lower protein levels in the stimulated tissue may correlate with a more ventricular rather than a nodal phenotype. The metabolic protein peroxisome proliferator activated receptor α (PPARα) was also more highly expressed (but not significantly) in Stretched+22V hCMPs than in Control hCMPs, which is consistent with the increase in fatty acid metabolism associated with CM maturation (Lopaschuk and Jaswal, 2010; Ellen Kreipke et al., 2016; Gentillon et al., 2019). A metabolic marker that showed consistent trends across both RNA and protein expression is the relative levels of Hexokinase (HK) one and 2. The protein ratios of HK2/1 in control and stimulated patches were found to be 0.64 ± 0.03 and 1.24 ± 0.08, respectively (Figure 5). This shift to the isoform that exhibits less glycolytic activity is a crucial indicator of the switch in metabolic activity in the more adult-like tissue (Calmettes et al., 2013; Fritz et al., 1999).

Multimodal stimulation increases ultrastructural elements

Images obtained via TEM (Figure 6A) confirmed that static stretching and electrical stimulation were associated with increases in the development of CM features (e.g., Z-lines, gap-junctions), as well as in the localization of mitochondria around contractile structures and a general broadening of the muscle fibers, particularly in Stretched+22V hCMPs. Sarcomeres were also significantly longer in Stretched (1.78 ± 0.06 μm), Stretched+15V (1.80 ± 0.04 μm), and Stretched+22V (1.91 ± 0.02 μm) hCMPs than in Control hCMPs (1.64 ± 0.02 μm), and although lengths did not differ significantly among the three groups that underwent the maturation protocols, measurements in the two electrically stimulated groups reached physiological relevance (Renshaw, 2008; Ribeiro et al., 2015).

DISCUSSION

Despite continued refinement of the techniques and materials used to generate engineered myocardial tissues, few studies have been conducted with hCMPs of clinically relevant dimensions. hCMPs with surface areas of 8 cm^2 have been investigated in a swine model of myocardial infarction (Gao et al., 2018), but even these relatively large patches were only ~1.25 mm thick. The hCMPs generated for this report exceeded 2.1 mm in thickness, and at least in principle, our lbl fabrication protocol could be used to produce even thicker hCMPs simply by depositing additional layers of

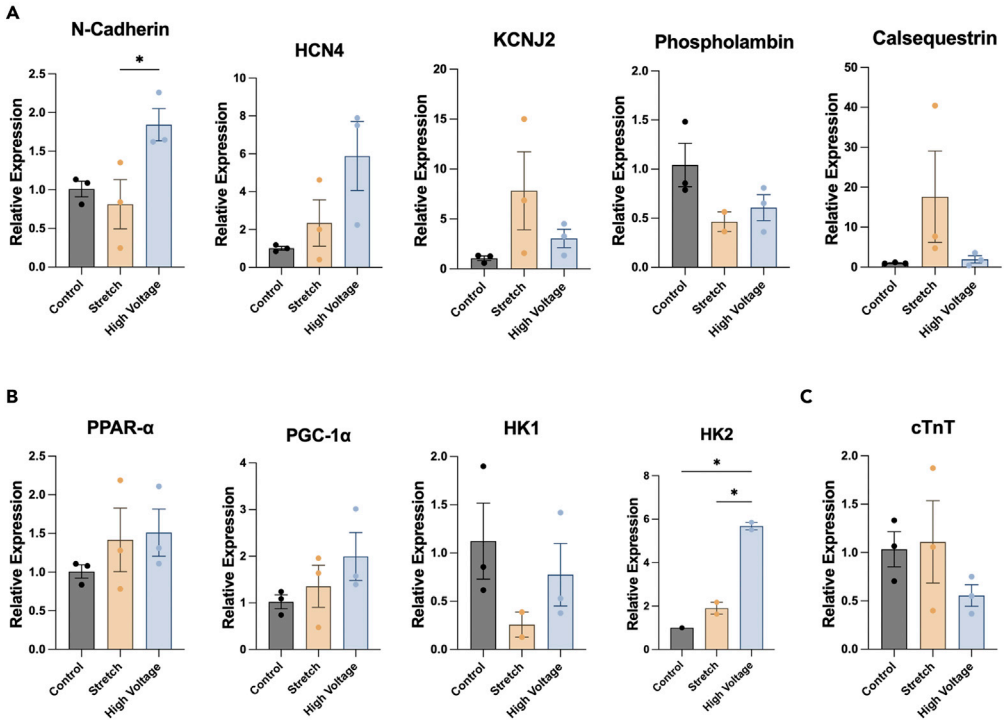

Figure 4. Static stretching with 22-V electrical stimulation was associated with more mature levels of CM gene expression

The abundance of mRNA for genes that contribute to the (A) calcium handling, (B) metabolic activity, and (C) structural function of CMs were evaluated in Control, Stretched, and Stretched+22V hCMPs via qPCR; results were normalized to the abundance of GAPDH mRNA in each sample (*$p < 0.05$; $n = 3$ per group).

hiPSC-CM–containing solution during manufacture. Nevertheless, the effectiveness of these multilayered constructs for cardiac therapy, disease modeling, and drug testing may still be limited by inadequate hiPSC-CM maturation.

In humans, the transition from a neonatal to adult-like CM phenotype typically occurs over a six- to 10-year period (Jiang et al., 2018), and some evidence suggests that several structural components of adult CMs require more than 30 days (Z-bands, I-bands, and A-bands) or nearly a year (M-bands) to fully develop in cultured hiPSC-CMs (Kamakura et al., 2013). Few (if any) practical applications of this promising technology can accommodate such long-term culture periods, but the results presented here demonstrate that the combination of static stretching with 22 V stimulation was associated with significantly more mature patterns of gene and protein expression, as well as morphological evidence of maturation, just 10 days later. Static stretching alone was sufficient to significantly promote sarcomere lengthening, but only the hCMPs matured via both stretching and electrical stimulation developed sarcomeres of physiologically relevant lengths, with sarcomeres surpassing 1.9 μm in length (Renshaw, 2008; Ribeiro et al., 2015).

Although electrical stimulation (Tandon et al., 2009, 2011; Nunes et al., 2013; Hirt et al., 2014; Eng et al., 2016) and mechanical stretching (both static and cyclical) (Tulloch et al., 2011; Hirt et al., 2012; Mihic et al., 2014; Rogers et al., 2016; Ruan et al., 2016; Leonard et al., 2018) are among the most frequently investigated methods for promoting the maturity of engineered myocardial tissues, a number of other factors can also influence hiPSC-CM maturation (Scuderi and Butcher, 2017; Jiang et al., 2018; Karbassi et al., 2020; Shadrin et al., 2017). CMs typically mature more efficiently when suspended in a three-dimensional matrix than when cultured in monolayers (Zhang et al., 2013; Jung et al., 2016; Mills et al., 2017; Hall and Ogle, 2018), and the matrix can be modified to optimize the stiffness of the substrate or to contain extracellular matrix (ECM) proteins that have been linked to CM maturation (Jiang et al., 2018). Furthermore, although CMs occupy 70–85% of the volume of mammalian hearts, they

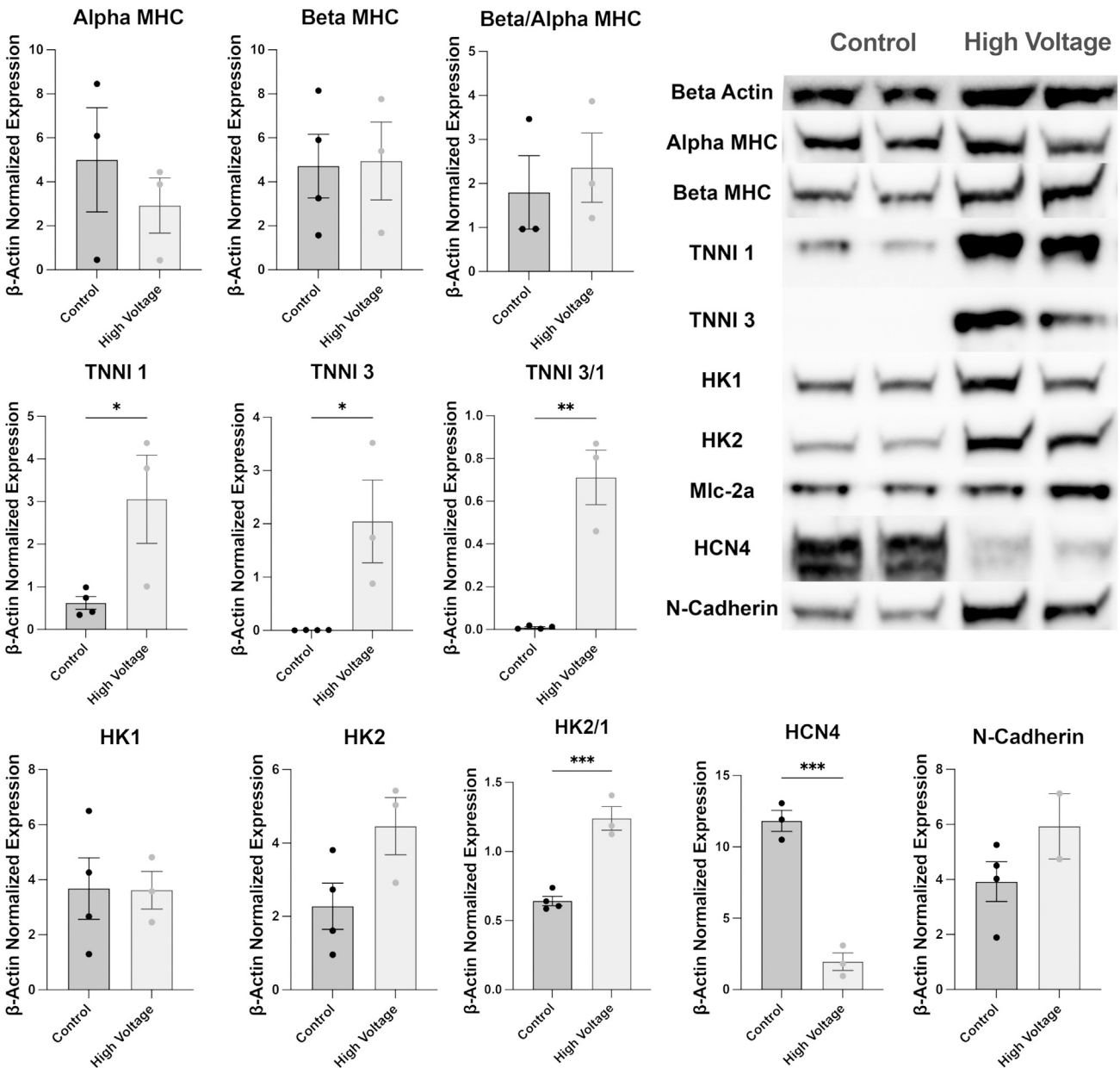

Figure 5. Static stretching with 22-V electrical stimulation increased protein expression of key cardiac maturation components

The abundance of protein for key structural and functional components were evaluated in Control and Stretched+22V hCMPs via western blotting; results were normalized to the abundance of Beta Actin protein in each sample (*$p < 0.05$; n = 3 per group).

comprise less than half the total number of cells (Zhou and Pu, 2016), and non-CM cell populations (e.g., fibroblasts, endothelial cells) can contribute to CM maturation via direct physical interactions and the production of paracrine factors (Jiang et al., 2018). Notably, the hCMPs generated for this report were composed primarily of hiPSC-CMs in an unmodified fibrin matrix; thus, hCMP maturation could likely be further enhanced by the inclusion of other cardiac cell types and ECM component optimization.

Although the data presented in the present works shows improved maturation over control tissues with dual stimulation techniques, the levels of individual markers had a high variability in their upregulation or downregulation across treatment groups. This would suggest that further optimization of the stimulation protocols is most likely necessary to achieve improvements in structural, electrical, and metabolic markers

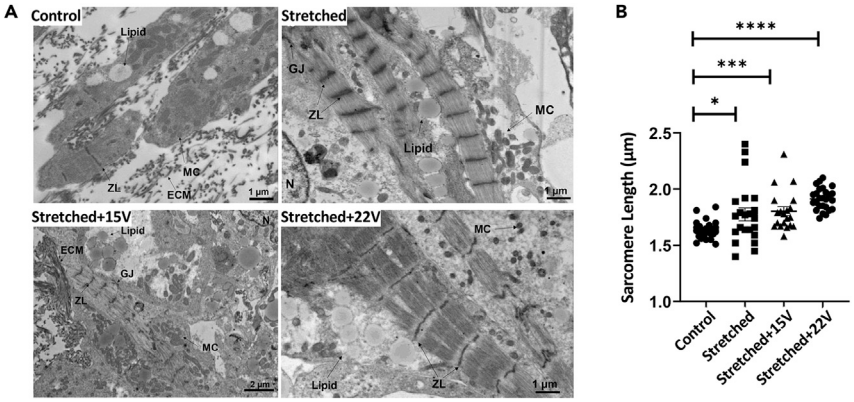

Figure 6. Static stretching with electrical stimulation was associated with structural maturation of CMs

(A and B) hCMP sections were imaged via TEM and analyzed qualitatively for functional components of the cardiomyocyte sarcomere (ECM: extracellular matrix, GJ: gap junction, MC: mitochondrion, N: nucleus, ZL: Z-line), and (B) sarcomere lengths were measured for each group (*$p < 0.05$, ***$p < 0.005$, ****$p < 0.0001$; images taken from at least three hCMP per group with n = 25 separate fields-of-view per group)

consistently across treated tissue. An additional limitation in the present work is the lack of adult myocardium as a control to provide an ideal target for maturation.

In conclusion, the results presented here demonstrate that our lbl fabrication protocol can be used to generate relatively thick (>2.1 mm) hCMPs from a mixture of hiPSC-CMs in a fibrin matrix, and that the maturity of the hiPSC-CMs can be dramatically increased by culturing the hCMP with static stretching and electrical stimulation for just ten days. These fabrication and maturation protocols are fully compatible with the production of hCMPs containing multiple cardiac-cell types, which may even more closely recapitulate the morphology and functional properties of adult myocardial tissue.

STAR★METHODS

Detailed methods are provided in the online version of this paper and include the following:

- KEY RESOURCES TABLE
- RESOURCE AVAILABILITY
  - Lead contact
  - Materials availability
  - Data and code availability
- EXPERIMENTAL MODEL AND SUBJECT DETAILS
  - hiPSC cell line
- METHOD DETAILS
  - Cell culture and characterization
  - hCMP manufacture
  - hCMP maturation
  - Sample preservation and staining
  - RNA isolation and analyses
  - Protein collection and analyses
  - Transmission electron microscope (TEM) imaging
  - Flow cytometry
- QUANTIFICATION AND STATISTICAL ANALYSIS
  - Statistical analyses

SUPPLEMENTAL INFORMATION

Supplemental information can be found online at https://doi.org/10.1016/j.isci.2022.103824.

ACKNOWLEDGMENTS

The authors would like to thank the High-Resolution Imaging Facility and the Comprehensive Flow Cytometry Core of the University of Alabama, Birmingham, for assistance with TEM sample preparation and cell purity analysis. We also appreciate Dr. Joel Berry who reviewed the manuscript. This study was supported in part by the National Institutes of Health (NIH) NHLBI grants RO1 HL114120, HL131017, HL149137, UO1 HL134764, NIGMS T32 GM008361, and NIBIB T32 EB023872.

AUTHOR CONTRIBUTIONS

Conceptualization, D.P. and W.L.; Methodology, D.P., A.K., and W.L.; Investigation, D.P., A.K., X.L., and W.L.; Visualization, A.K. and D.P.; Writing – Original Draft, D.P., A.K., and J.Z.; Writing – Review & Editing, A.K., D.P., and J.Z.; Funding Acquisition, J.Z.; Resources, J.Z.; Supervision, J.Z.

DECLARATION OF INTERESTS

The authors declare no competing interests.

Received: August 9, 2021
Revised: November 23, 2021
Accepted: January 24, 2022
Published: March 18, 2022

REFERENCES

Allen, D.L., and Leinwand, L.A. (2001). Postnatal myosin heavy chain isoform expression in normal mice and mice null for IIb or IId myosin heavy chains. Dev. Biol. *229*, 383–395. https://doi.org/10.1006/dbio.2000.9974.

Argentati, C., Tortorella, I., Bazzucchi, M., Morena, F., and Martino, S. (2020). Harnessing the potential of stem cells for disease modeling: progress and promises. J. Pers Med. *10*, 8. https://doi.org/10.3390/jpm10010008.

Bartos, D.C., Grandi, E., and Ripplinger, C.M. (2015). Ion channels in the heart. Compr. Physiol. *5*, 1423–1464. https://doi.org/10.1002/cphy.c140069.

Bedada, F.B., Chan, S.S.-K., Metzger, S.K., Zhang, L., Zhang, J., Garry, D.J., Kamp, T.J., Kyba, M., and Metzger, J.M. (2014). Acquisition of a quantitative, stoichiometrically conserved ratiometric marker of maturation status in stem cell-derived cardiac myocytes. Stem Cell Rep. *3*, 594–605. https://doi.org/10.1016/j.stemcr.2014.07.012.

Benam, K.H., Dauth, S., Hassell, B., Herland, A., Jain, A., Jang, K.J., et al. (2015). Engineered in vitro disease models. Annu. Rev. Pathol. *10*, 195–262. https://doi.org/10.1146/annurev-pathol-012414-040418.

Berger, H.J., Prasad, S.K., Davidoff, A.J., Pimental, D., Ellingsen, O., Marsh, J.D., Smith, T.W., and Kelly, R.A. (1994). Continual electric field stimulation preserves contractile function of adult ventricular myocytes in primary culture. Am. J. Physiol. *266*, H341–H349. https://doi.org/10.1152/ajpheart.1994.266.1.H341.

Bian, W., Badie, N., Himel, H.D., and Bursac, N. (2014). Robust T-tubulation and maturation of cardiomyocytes using tissue-engineered epicardial mimetics. Biomaterials *35*, 3819–3828. https://doi.org/10.1016/j.biomaterials.2014.01.045.

Buccitelli, C., and Selbach, M. (2020). mRNAs, proteins and the emerging principles of gene expression control. Nat. Rev. Genet. *21*, 630–644. https://doi.org/10.1038/s41576-020-0258-4.

Burridge, P.W., Matsa, E., Shukla, P., Lin, Z.C., Churko, J.M., Ebert, A.D., Lan, F., Diecke, S., Huber, B., Mordwinkin, N.M., et al. (2014). Chemically defined generation of human cardiomyocytes. Nat. Methods *11*, 855–860. https://doi.org/10.1038/nmeth.2999.

Calmettes, G., John, S.A., Weiss, J.N., and Ribalet, B. (2013). Hexokinase–mitochondrial interactions regulate glucose metabolism differentially in adult and neonatal cardiac myocytes. J. Gen. Physiol. *142*, 425–436. https://doi.org/10.1085/jgp.201310968.

Darche, F.F., Rivinius, R., Köllensperger, E., Leimer, U., Germann, G., Seckinger, A., Hose, D., Schröter, J., Bruehl, C., Draguhn, A., et al. (2019). Pacemaker cell characteristics of differentiated and HCN4-transduced human mesenchymal stem cells. Life Sci. *232*, 116620. https://doi.org/10.1016/j.lfs.2019.116620.

Ellen Kreipke, R., Wang, Y., Miklas, J.W., Mathieu, J., and Ruohola-Baker, H. (2016). Metabolic remodeling in early development and cardiomyocyte maturation. Semin. Cell Dev Biol *52*, 84–92. https://doi.org/10.1016/j.semcdb.2016.02.004.

Eng, G., Lee, B.W., Protas, L., Gagliardi, M., Brown, K., Kass, R.S., Keller, G., Robinson, R.B., and Vunjak-Novakovic, G. (2016). Autonomous beating rate adaptation in human stem cell-derived cardiomyocytes. Nat. Commun. *7*, 10312. https://doi.org/10.1038/ncomms10312.

Fritz, H.L., Smoak, I.W., and Branch, S. (1999). Hexokinase I expression and activity in embryonic mouse heart during early and late organogenesis. Histochem. Cell Biol *112*, 359–365. https://doi.org/10.1007/s004180050417.

Gao, L., Gregorich, Z.R., Zhu, W., Mattapally, S., Oduk, Y., Lou, X., Kannappan, R., Borovjagin, A.V., Walcott, G.P., Pollard, A.E., et al. (2018). Large cardiac muscle patches engineered from human induced-pluripotent stem cell-derived cardiac cells improve recovery from myocardial infarction in swine. Circulation *137*, 1712–1730. https://doi.org/10.1161/CIRCULATIONAHA.117.030785.

Gentillon, C., Li, D., Duan, M., Yu, W.M., Preininger, M.K., Jha, R., Rampoldi, A., Saraf, A., Gibson, G.C., Qu, C.K., et al. (2019). Targeting HIF-1alpha in combination with PPARalpha activation and postnatal factors promotes the metabolic maturation of human induced pluripotent stem cell-derived cardiomyocytes. J. Mol. Cell Cardiol *132*, 120–135. https://doi.org/10.1016/j.yjmcc.2019.05.003.

Goldfracht, I., Protze, S., Shiti, A., Setter, N., Gruber, A., Shaheen, N., Nartiss, Y., Keller, G., and Gepstein, L. (2020). Generating ring-shaped engineered heart tissues from ventricular and atrial human pluripotent stem cell-derived cardiomyocytes. Nat. Commun. *11*, 75. https://doi.org/10.1038/s41467-019-13868-x.

Grant, A.O. (2009). Cardiac ion channels. Circ. Arrhythm Electrophysiol. *2*, 185–194. https://doi.org/10.1161/CIRCEP.108.789081.

Hall, M.L., and Ogle, B.M. (2018). Cardiac extracellular matrix modification as a therapeutic approach. Adv. Exp. Med. Biol. *1098*, 131–150. https://doi.org/10.1007/978-3-319-97421-7_7.

Hartung, T. (2008). Thoughts on limitations of animal models. Parkinsonism Relat. Disord. *14* (*Suppl 2*), S81–S83. https://doi.org/10.1016/j.parkreldis.2008.04.003.

Hirt, M.N., Boeddinghaus, J., Mitchell, A., Schaaf, S., Bornchen, C., Muller, C., Schulz, H.,

Hubner, N., Stenzig, J., Stoehr, A., et al. (2014). Functional improvement and maturation of rat and human engineered heart tissue by chronic electrical stimulation. J. Mol. Cell Cardiol *74*, 151–161. https://doi.org/10.1016/j.yjmcc.2014.05.009.

Hirt, M.N., Sorensen, N.A., Bartholdt, L.M., Boeddinghaus, J., Schaaf, S., Eder, A., Vollert, I., Stöhr, A., Schulze, T., Witten, A., et al. (2012). Increased afterload induces pathological cardiac hypertrophy: a new in vitro model. Basic Res. Cardiol. *107*, 307. https://doi.org/10.1007/s00395-012-0307-z.

Ivester, C.T., Kent, R.L., Tagawa, H., Tsutsui, H., Imamura, T., Cooper, G., 4th, and McDermott, P.J. (1993). Electrically stimulated contraction accelerates protein synthesis rates in adult feline cardiocytes. Am. J. Physiol. *265*, H666–H674. https://doi.org/10.1152/ajpheart.1993.265.2.H666.

Jiang, Y., Park, P., Hong, S.M., and Ban, K. (2018). Maturation of cardiomyocytes derived from human pluripotent stem cells: current strategies and limitations. Mol. Cells *41*, 613–621. https://doi.org/10.14348/molcells.2018.0143.

Jung, J.P., Bhuiyan, D.B., and Ogle, B.M. (2016). Solid organ fabrication: comparison of decellularization to 3D bioprinting. Biomater. Res. *20*, 27. https://doi.org/10.1186/s40824-016-0074-2.

Kamakura, T., Makiyama, T., Sasaki, K., Yoshida, Y., Wuriyanghai, Y., Chen, J., Hattori, T., Ohno, S., Kita, T., Horie, M., et al. (2013). Ultrastructural maturation of human-induced pluripotent stem cell-derived cardiomyocytes in a long-term culture. Circ. J. *77*, 1307–1314. https://doi.org/10.1253/circj.cj-12-0987.

Karbassi, E., Fenix, A., Marchiano, S., Muraoka, N., Nakamura, K., Yang, X., and Murry, C.E. (2020). Cardiomyocyte maturation: advances in knowledge and implications for regenerative medicine. Nat. Rev. Cardiol. *17*, 341–359. https://doi.org/10.1038/s41569-019-0331-x.

Kato, S., Ivester, C.T., Cooper, G.t., Zile, M.R., and McDermott, P.J. (1995). Growth effects of electrically stimulated contraction on adult feline cardiocytes in primary culture. Am. J. Physiol. *268*, H2495–H2504. https://doi.org/10.1152/ajpheart.1995.268.6.H2495.

Leonard, A., Bertero, A., Powers, J.D., Beussman, K.M., Bhandari, S., Regnier, M., Murry, C.E., and Sniadecki, N.J. (2018). Afterload promotes maturation of human induced pluripotent stem cell derived cardiomyocytes in engineered heart tissues. J. Mol. Cell Cardiol *118*, 147–158. https://doi.org/10.1016/j.yjmcc.2018.03.016.

Li, M., Kanda, Y., Ashihara, T., Sasano, T., Nakai, Y., Kodama, M., Hayashi, E., Sekino, Y., Furukawa, T., and Kurokawa, J. (2017). Overexpression of KCNJ2 in induced pluripotent stem cell-derived cardiomyocytes for the assessment of QT-prolonging drugs. J. Pharmacol. Sci. *134*, 75–85. https://doi.org/10.1016/j.jphs.2017.05.004.

Lian, X., Zhang, J., Azarin, S.M., Zhu, K., Hazeltine, L.B., Bao, X., Hsiao, C., Kamp, T.J., and Palecek, S.P. (2013). Directed cardiomyocyte differentiation from human pluripotent stem cells by modulating Wnt/beta-catenin signaling under fully defined conditions. Nat. Protoc. *8*, 162–175. https://doi.org/10.1038/nprot.2012.150.

Liu, J., Lieu, D.K., Siu, C.W., Fu, J.D., Tse, H.F., and Li, R.A. (2009). Facilitated maturation of Ca2+ handling properties of human embryonic stem cell-derived cardiomyocytes by calsequestrin expression. Am. J. Physiol. Cell Physiol *297*, C152–C159. https://doi.org/10.1152/ajpcell.00060.2009.

Lopaschuk, G.D., and Jaswal, J.S. (2010). Energy metabolic phenotype of the cardiomyocyte during development, differentiation, and postnatal maturation. J. Cardiovasc. Pharmacol. *56*, 130–140. https://doi.org/10.1097/FJC.0b013e3181e74a14.

Lou, X., Zhao, M., Fan, C., Fast, V.G., Valarmathi, M.T., Zhu, W., and Zhang, J. (2020). N-cadherin overexpression enhances the reparative potency of human-induced pluripotent stem cell-derived cardiac myocytes in infarcted mouse hearts. Cardiovasc. Res. *116*, 671–685. https://doi.org/10.1093/cvr/cvz179.

Mihic, A., Li, J., Miyagi, Y., Gagliardi, M., Li, S.H., Zu, J., Weisel, R.D., Keller, G., and Li, R.K. (2014). The effect of cyclic stretch on maturation and 3D tissue formation of human embryonic stem cell-derived cardiomyocytes. Biomaterials *35*, 2798–2808. https://doi.org/10.1016/j.biomaterials.2013.12.052.

Mills, R.J., Titmarsh, D.M., Koenig, X., Parker, B.L., Ryall, J.G., Quaife-Ryan, G.A., Voges, H.K., Hodson, M.P., Ferguson, C., Drowley, L., et al. (2017). Functional screening in human cardiac organoids reveals a metabolic mechanism for cardiomyocyte cell cycle arrest. Proc. Natl. Acad. Sci. U S A. *114*, E8372–E8381. https://doi.org/10.1073/pnas.1707316114.

Molinari, E., and Sayer, J.A. (2020). Disease modeling to understand the pathomechanisms of human genetic kidney disorders. Clin. J. Am. Soc. Nephrol. *15*, 855–872. https://doi.org/10.2215/CJN.08890719.

Ng, S.Y., Wong, C.K., and Tsang, S.Y. (2010). Differential gene expressions in atrial and ventricular myocytes: insights into the road of applying embryonic stem cell-derived cardiomyocytes for future therapies. Am. J. Physiol. Cell Physiol *299*, C1234–C1249. https://doi.org/10.1152/ajpcell.00402.2009.

Nunes, S.S., Miklas, J.W., Liu, J., Aschar-Sobbi, R., Xiao, Y., Zhang, B., Jiang, J., Massé, S., Gagliardi, M., Hsieh, A., et al. (2013). Biowire: a platform for maturation of human pluripotent stem cell-derived cardiomyocytes. Nat. Methods *10*, 781–787. https://doi.org/10.1038/nmeth.2524.

Pretorius, D., Kahn-Krell, A.M., LaBarge, W.C., Lou, X., Kannappan, R., Pollard, A.E., Fast, V.G., Berry, J.L., Eberhardt, A.W., and Zhang, J. (2020). Fabrication and characterization of a thick, viable bi-layered stem cell-derived surrogate for future myocardial tissue regeneration. Biomed. Mater. *16*. https://doi.org/10.1088/1748-605X/abc107.

Pretorius, D., Kahn-Krell, A.M., Lou, X., Fast, V.G., Berry, J.L., Kamp, T.J., and Zhang, J. (2021). Layer-by-layer fabrication of large and thick human cardiac muscle patch constructs with superior electrophysiological properties. Front Cell Dev Biol *9*, 670504. https://doi.org/10.3389/fcell.2021.670504.

Reiser, P.J., Portman, M.A., Ning, X.H., and Schomisch Moravec, C. (2001). Human cardiac myosin heavy chain isoforms in fetal and failing adult atria and ventricles. Am. J. Physiol. Heart Circ. Physiol. *280*, H1814–H1820. https://doi.org/10.1152/ajpheart.2001.280.4.H1814.

Renshaw, A. (2008). Rubin's pathology. Clinicopathologic foundations of medicine. Adv. Anat. Pathol. *15*, 125.

Ribeiro, M.C., Tertoolen, L.G., Guadix, J.A., Bellin, M., Kosmidis, G., D'Aniello, C., Monshouwer-Kloots, J., Goumans, M.J., Wang, Y.L., Feinberg, A.W., et al. (2015). Functional maturation of human pluripotent stem cell derived cardiomyocytes in vitro–correlation between contraction force and electrophysiology. Biomaterials *51*, 138–150. https://doi.org/10.1016/j.biomaterials.2015.01.067.

Rogers, A.J., Fast, V.G., and Sethu, P. (2016). Biomimetic cardiac tissue model enables the adaption of human induced pluripotent stem cell cardiomyocytes to physiological hemodynamic loads. Anal Chem. *88*, 9862–9868. https://doi.org/10.1021/acs.analchem.6b03105.

Ronaldson-Bouchard, K., Ma, S.P., Yeager, K., Chen, T., Song, L., Sirabella, D., Morikawa, K., Teles, D., Yazawa, M., and Vunjak-Novakovic, G. (2018). Advanced maturation of human cardiac tissue grown from pluripotent stem cells. Nature *556*, 239–243. https://doi.org/10.1038/s41586-018-0016-3.

Ruan, J.L., Tulloch, N.L., Razumova, M.V., Saiget, M., Muskheli, V., Pabon, L., Reinecke, H., Regnier, M., and Murry, C.E. (2016). Mechanical stress conditioning and electrical stimulation promote contractility and force maturation of induced pluripotent stem cell-derived human cardiac tissue. Circulation *134*, 1557–1567. https://doi.org/10.1161/CIRCULATIONAHA.114.014998.

Scuderi, G.J., and Butcher, J. (2017). Naturally engineered maturation of cardiomyocytes. Front Cell Dev Biol *5*, 50. https://doi.org/10.3389/fcell.2017.00050.

Shadrin, I.Y., Allen, B.W., Qian, Y., Jackman, C.P., Carlson, A.L., Juhas, M.E., and Bursac, N. (2017). Cardiopatch platform enables maturation and scale-up of human pluripotent stem cell-derived engineered heart tissues. Nat. Commun. *8*, 1825. https://doi.org/10.1038/s41467-017-01946-x.

Tandon, N., Cannizzaro, C., Chao, P.H., Maidhof, R., Marsano, A., Au, H.T., Radisic, M., and Vunjak-Novakovic, G. (2009). Electrical stimulation systems for cardiac tissue engineering. Nat. Protoc. *4*, 155–173. https://doi.org/10.1038/nprot.2008.183.

Tandon, N., Marsano, A., Maidhof, R., Wan, L., Park, H., and Vunjak-Novakovic, G. (2011). Optimization of electrical stimulation parameters for cardiac tissue engineering. J. Tissue Eng. Regen. Med. *5*. e115–125. https://doi.org/10.1002/term.377.

Tulloch, N.L., Muskheli, V., Razumova, M.V., Korte, F.S., Regnier, M., Hauch, K.D., Pabon, L.,

Reinecke, H., and Murry, C.E. (2011). Growth of engineered human myocardium with mechanical loading and vascular coculture. Circ. Res. *109*, 47–59. https://doi.org/10.1161/CIRCRESAHA.110.237206.

Ye, L., Chang, Y.H., Xiong, Q., Zhang, P., Zhang, L., Somasundaram, P., Lepley, M., Swingen, C., Su, L., Wendel, J.S., et al. (2014). Cardiac repair in a porcine model of acute myocardial infarction with human induced pluripotent stem cell-derived cardiovascular cells. Cell Stem Cell *15*, 750–761. https://doi.org/10.1016/j.stem.2014.11.009.

Zhang, D., Shadrin, I.Y., Lam, J., Xian, H.Q., Snodgrass, H.R., and Bursac, N. (2013). Tissue-engineered cardiac patch for advanced functional maturation of human ESC-derived cardiomyocytes. Biomaterials *34*, 5813–5820. https://doi.org/10.1016/j.biomaterials.2013.04.026.

Zhang, L., Guo, J., Zhang, P., Xiong, Q., Wu, S.C., Xia, L., Roy, S.S., Tolar, J., O'Connell, T.D., Kyba, M., et al. (2014). Derivation and high engraftment of patient-specific cardiomyocyte sheet using induced pluripotent stem cells generated from adult cardiac fibroblast. Circ. Hear Fail. *8*, 156–166. https://doi.org/10.1161/circheartfailure.114.001317.

Zhou, P., and Pu, W.T. (2016). Recounting cardiac cellular composition. Circ. Res. *118*, 368–370. https://doi.org/10.1161/CIRCRESAHA.116.308139.

Zhu, W., Gao, L., and Zhang, J. (2017). Pluripotent stem cell derived cardiac cells for myocardial repair. J. Vis. Exp. 55142. https://doi.org/10.3791/55142.

STAR★METHODS

KEY RESOURCES TABLE

REAGENT or RESOURCE	SOURCE	IDENTIFIER
Antibodies		
Recombinant Anti-Cardiac Troponin T antibody [EPR3695]	Abcam	RRID: AB_2050427
Monoclonal Anti-α-Actinin (Sarcomeric)	Sigma	RRID: AB_476766
Troponin T, Cardiac Isoform Ab-1, Mouse Monoclonal Antibody	Thermo Fisher Scientific	Cat#MS-295-P; RRID: AB_61806
Zenon™ Mouse IgG_1 Labeling Kit	Invitrogen	Cat#Z-25002; RRID: AB_2736941
Anti-Troponin I Type 3 Rabbit Polyclonal Antibody	Proteintech	Cat# 21652-1-AP; RRID: AB_2878898
Anti-Troponin I Type 1 Rabbit Polyclonal Antibody	Proteintech	Cat# 16102-1-AP; RRID: AB_2206103
Anti-HK1 Rabbit Polyclonal Antibody	Proteintech	Cat# 19662-1-AP; RRID: AB_10859778
HK2 Monoclonal antibody	Proteintech	Cat# 66974-1-Ig; RRID: AB_2882294
Anti-HCN4 Rabbit Polyclonal Antibody	Proteintech	Proteintech Cat# 55224-1-AP; RRID: AB_11182714
Anti-CDH2 Rabbit Polyclonal Antibody	Proteintech	Cat# 22018-1-AP; RRID: AB_2813891
Anti-MYH6 Rabbit Polyclonal Antibody	Proteintech	Cat# 22281-1-AP; RRID: AB_2736822
MYH7 Rabbit anti-Human, Mouse	Proteintech	Cat# 22280-1-AP; RRID: AB_2736821
Myl7 Polyclonal Antibody	Thermo Fisher Scientific	Cat# PA5-30789; RRID: AB_2548263
β-Actin (8H10D10) Mouse mAb antibody	Cell Signaling Technology	Cat# 3700; RRID: AB_2242334
Anti-mouse IgG, HRP-linked Antibody	Cell Signaling Technology	Cat# 7076; RRID: AB_330924
Anti rabbit IgG, HRP linked Antibody	Cell Signaling Technology	Cat# 7074; RRID: AB_2099233
Goat anti-Mouse IgG (H+L) Highly Cross-Adsorbed Secondary Antibody, Alexa Fluor Plus 555	Invitrogen	Cat# A32727; RRID: AB_2633276
Goat anti-Rabbit IgG (H+L) Highly Cross-Adsorbed Secondary Antibody, Alexa Fluor Plus 488	Invitrogen	Cat# A32731; RRID: AB_2633280
4′ 6-DIAMIDINO-2-PHENYINDOLE DILACTATE	Sigma-Aldrich	Cat# D9564
Chemicals, peptides, and recombinant proteins		
Fibrinogen from bovine plasma	Sigma-Aldrich	Cat#F8630
6-Aminocaproic acid	Acros Organics	Cat#AC103301000
Fetal Bovine Serum	Bio-Techne	Cat#S11150
16% Formaldehyde (w/v), Methanol-free	Thermo Scientific	Cat#28906
Tissue-Plus™ O.C.T. Compound	Fisher Scientific	Cat#23-730-571
Donkey Serum	Sigma-Aldrich	Cat#S30-100ML
Tween™ 20	Fisher Scientific	Cat#BP337-100
Bovine Serum Albumin	Sigma-Aldrich	Cat#A7906
Triton™ X-100	Fisher Scientific	Cat#BP151-100
Sodium Azide	Sigma-Aldrich	Cat#S2002
Vectashield	Vector Laboratories	Cat# H-1000; RRID: AB_2336789
TRIzol™ Reagent	Thermo Fisher Scientific	Cat#15596018
EMS Glutaraldehyde 3% Aqueous	Electron Microscopy Sciences	Cat#16537-20-S
Critical commercial assays		
Direct-zol RNA MiniPrep PlusDirect-zol RNA MiniPrep Plus	Zymo Research	Cat#R2072
SuperScript IV VILO Master Mix	Thermo Fisher Scientific	Cat#11756500
PowerUp SYBR Green Master Mix	Applied Biosystems	Cat#A25741
Expressplus™ PAGE Gel 4-20%, 15 wells	GenScript	Cat# M42015
Trans-Blot ® Turbo™ RTA Midi Nitrocellulose Transfer Kit	Bio-Rad	Cat# 1704271

(*Continued on next page*)

Continued

REAGENT or RESOURCE	SOURCE	IDENTIFIER
Deposited data		
Raw Data	Mendeley Data	https://doi.org/10.17632/h59p23ct7d
Experimental Models: Cell Lines		
lzhipsc5	Zhang Lab	lzhipsc5
Oligonucleotides		
qPCR Primers	See Table S1 for a list of oligonucleotides.	N/A
Software and algorithms		
Prism 9	Graphpad	RRID: SCR_002798
Flowjo	BD Biosciences	RRID: SCR_008520
ImageLab	Bio-Rad	RRID: SCR_014210

RESOURCE AVAILABILITY

Lead contact

Further information and requests for resources and reagents should be directed to and will be fulfilled by the lead contact, Jianyi Zhang (jayzhang@uab.edu).

Materials availability

This study did not generate new unique reagents.

Data and code availability

All datasets are included in the present article and supplementary information. This paper does not report original code. Raw data from Figures 3, 4, and 5 were deposited on Mendeley Data: https://doi.org/10.17632/h59p23ct7d. Any additional information required to reanalyze the data reported in this paper is available from the lead contact upon request.

EXPERIMENTAL MODEL AND SUBJECT DETAILS

hiPSC cell line

We previously reprogrammed and characterized the LZ-hiPSC5 hiPSC line from deidentified human cardiac fibroblast samples from consenting donors (Zhang et al., 2014). Line lzhiPSC5 was reprogrammed with CytoTune-iPS 2.0 Sendai Reprogramming Kits by Dr. Liying Zhang in the laboratory of Dr. Jianyi Zhang from the University of Minnesota donor fibroblasts. lzhiPSC5 was previously comprehensively characterized for pluripotency (immunofluorescence, RT-PCR), G-band karyotype, teratoma formation, and multi-lineage differentiation. G-band karyotype was performed by the University of Minnesota's Cytogenics Core Laboratory.

METHOD DETAILS

Cell culture and characterization

hiPSCs were reprogrammed from human cardiac fibroblasts and maintained under optimized conditions (Zhang et al., 2014; Zhu et al., 2017) in mTeSR Plus (STEMCell) maintenance media on 6-well plates coated with Geltrex (Gibco). hiPSC-CM differentiation was conducted as previously reported (Lian et al., 2013; Burridge et al., 2014; Ye et al., 2014). Briefly, when iPSCs reached 80-100% confluency, referred to as day 0, media was changed to 2.5 mL RPMI 1640 with B27 without insulin (RPMI/B27-) (Gibco) supplemented with 10 μM CHIR99021. Subsequently, on days 1, 3, and 5 media was changed to 3 mL RPMI/B27- and supplemented with 5 μM IWR on day 3. Media was changed to RPMI 1640 with B27 with insulin (RPMI/B27+) on day 7. Spontaneous contractions were typically observed 7 to 10 days after differentiation was initiated, and the number of beating cells continued to increase until day 12. The differentiated hiPSC-CMs were purified by culturing them in the absence of glucose (RPMI 1640 without glucose, supplemented with sodium

DL-lactate and B27$^+$, Gibco) for 3-6 days beginning on day 9; at least 95% of the purified cells expressed cardiac troponin T (cTnT) as shown in Figure S1. Cells were maintained in RPMI/B27+ until used for fabrication and dissociated using STEMdiff™ Cardiomyocyte Dissociation media as needed.

hCMP manufacture

Petri dishes (BioLite Cell Culture Treated Dishes, Thermo Scientific) were coated with 5% pluronic F-68 solution (Gibco) and incubated overnight at 4 °C; then, the pluronic solution was removed, and a sterile, modified Delrin frame (1 cm × 2 cm) was secured to the dish with 2% agarose. hCMPs were assembled in three layers over a three-day period (one layer per day). Each layer was generated by depositing 600 μL of an hiPSC-CM–containing fibrin solution (Gao et al., 2018; Pretorius et al., 2020, 2021) (10 × 10^6 cells/mL) into the frame (Pretorius et al., 2020, 2021); then, after fibrin polymerization, the layer was cultured in STEMdiff Cardiomyocyte Support Medium with 2 mg/mL ε-aminocaproic acid overnight at 37 °C and 5% CO_2; the procedure was repeated twice to form the second and third layers. After the third cell layer was generated, the frame containing the engineered tissue was lifted off of the petri dish and placed on a custom-cut polydimethylsiloxane (PDMS) platform; then, the hCMP was cultured in fresh culture medium consisting of 2% fetal bovine serum (FBS), 2% B27$^+$ (Gibco), and 2 mg/mL ε-aminocaproic acid in RPMI (Gibco) for one week before the maturation protocols were initiated.

hCMP maturation

Maturation was induced by stretching the hCMPs between two parallel lines of medical-grade stainless-steel needles (180 μm diameter, 13 mm long and then culturing the hCMPs with or without electrical stimulation (15V or 22V) for 10 days. Each line was composed of 6 needles positioned at 1-mm intervals, and the lines were fixed 1.8 mm apart on a PDMS base. Engineered constructs were mounted onto the stainless-steel needles, at a fixed height of 9 mm from the PDMS base. The taut 2 cm long tissues were lowered onto and embedded on top of the needle array, and subsequently released from the frames that they had been cultured in. Chronic biphasic electrical stimulation (C-Pace, IonOptix) was performed at 15V or 22V in 2-ms pulses at a frequency of 2 Hz, and the electrical field was positioned perpendicular to the direction of stretching (Ivester et al., 1993; Berger et al., 1994; Kato et al., 1995).

Sample preservation and staining

Tissue samples were fixed in 4% formaldehyde (Pierce, Thermo Scientific, # 28906) for 1 hour and then embedded in optimal cutting temperature compound (OCT compound, Fisher Health Care, USA). Frozen sections were cut at 10 μm thickness then blocked; permeabilized in 10% donkey serum, 10% Tween-20, 3% bovine serum albumin (BSA), 0.05% Triton-X, and 0.02% sodium azide in PBS; incubated with primary antibodies (Table S1); washed three times (10 minutes per wash) in PBS+Tween; labeled with fluorescent secondary antibodies and DAPI; and washed. Labeled samples were covered with VECTASHIELD Antifade Mounting Medium, and then visualized via confocal laser scanning (Olympus FV3000 confocal microscope).

RNA isolation and analyses

Samples were suspended in TRIZOL (Invitrogen) and homogenized; then, RNA extraction was performed with Direct-zol RNA MiniPrep Plus (Zymo Research Corporation) as directed by the manufacturer's protocol. RNA concentrations were measured with a Nanodrop device, and 1 μg of RNA was converted into complementary DNA (cDNA) via reverse transcription with SuperScript IV VILO Master Mix (Thermo Fisher Scientific). The cDNA was diluted to a final concentration of 5 ng/μL, and quantitative polymerase chain reaction (PCR) was performed on a QuantStudio 3 real-time PCR system with PowerUp SYBR Green Master Mix (Thermo Fisher Scientific) and the primers listed in Table S2. Measurements were normalized to the expression of glyceraldehyde phosphate dehydrogenase (GAPDH) for each sample.

Protein collection and analyses

Samples were lysed with 500 μL RIPA Buffer (Sigma-Aldrich) premixed with Proteinase Inhibitor (Fisher Scientific). Complete digestion was achieved by 3 successive 3 second pulses of sonication at 50% power. Following centrifugation sample concentration was determined by performing Pierce™ BCA Protein Assay (Thermo Fisher Scientific) according to the manufacturers protocol. Loading samples were prepared by combining 4x Laemmli Sample Buffer (Bio-Rad), 2-Mercaptoethanol, and 200 μg of each sample in a final volume of 200 μL. An Expressplus™ PAGE Gel 4-20% (GenScript) was prepare and loaded with 35 μL of each sample then run at 200V for 30 minutes. Proteins were transferred to a nitrocellulose membrane using the

Trans-Blot ® Turbo™ (Bio-Rad) System then blots were blocked with 5% Non-Fat Dry Milk in TBST (Santa Cruz Biotechnology) for 30 min. Samples were incubated in primary antibody (Table S1) overnight at 4 °C then secondary antibody at room temperature for 1 hr. Chemiluminescent Substrate was added to each blot for 5 min prior to imaging on a ChemiDoc Touch Imager (Bio-Rad). Relative protein levels were determined via quantification in ImageLab (Bio-Rad) and normalized to the Beta-Actin band.

Transmission electron microscope (TEM) imaging

Samples were fixed in 2.5% glutaraldehyde solution for 1 hour at 4 °C and then delivered to the High-Resolution Imaging Facility at the University of Alabama, Birmingham, for TEM imaging. Sample blocks were sectioned with a diamond knife, mounted, and imaged with a Tecnai Spirit T12 Transmission Electron Microscope.

Flow cytometry

Cardiomyocytes were dissociated using Cardiomyocyte Dissociation Reagent (Stem Cell) for 8 min at 37 °C then physically dislodged by pipetting. Single cells were fixed in 4% Paraformaldehyde (Thermo Fisher Scientific) for 15 min then permeabilized in 0.1% Triton-X and blocked with 4% BSA/4% FBS sequentially for 30 minutes each. Cells were stained with Anti-Troponin T antibody conjugated using Zenon Alexa-488 (Thermo Fisher Scientific) for 1 hour at room temperature then analyzed on the Attune Nxt Flow Cytometer (Thermo Fisher Scientific).

QUANTIFICATION AND STATISTICAL ANALYSIS

Statistical analyses

Results are reported as mean ± standard error of the mean (mean ± SEM), and statistical analyses were performed with GraphPad Prism9 software. Differences between two groups were evaluated via the Student's Two-Tailed t-Test, and differences among three or more groups or for repeated measurements were evaluated via ANOVA or repeated ANOVA with the Tukey post-hoc test. A p-value of less than 0.05 was considered statistically significant.